Flow boiling of R1233zd(E) in a 3 mm vertical tube at moderate and high reduced pressures

Michał Pysz, Dariusz Mikielewicz [*]

Gdańsk University of Technology, Faculty of Mechanical Engineering and Ship Technology, ul. Narutowicza 11/12, 80-233 Gdańsk, Poland

ARTICLE INFO

ABSTRACT

The results of flow boiling of R1233zd(E) in a 3 mm vertical stainless steel tube are presented at moderate and high saturation temperatures. Integral flow characteristics in the form of pressure drop and heat transfer coefficient are discussed for saturation temperatures ranging from 115 to 145 °C (corresponding reduced pressures from 0.2 to 0.7), mass velocity of 800 kg/m²s and heat flux of 20 kW/m². All of the obtained heat transfer trends initially decrease with vapor quality and then do not change or increase with vapor quality. The decrease is connected to the dominance of the nucleate boiling phenomenon. The subsequent increase in heat transfer indicates the increased effect of convective boiling. The rate of the increase depends on the value of reduced pressure (the smaller the reduced pressure the higher the rate). The obtained data have been compared with the predictions of the in-house model and some well-known two-phase flow correlations. The in-house model predictions presented the highest accuracy, with MAPE equal to 23.17 % for R1233zd(E) and 19.23 % for R245fa (data from literature).

1. Introduction

Pressure drop and heat transfer in flow boiling and flow condensation close to thermodynamic critical point attract attention of researchers from the point of view of new applications such as for example heat exchangers of the organic Rankine cycle (ORC) or high temperature heat pumps (HTHP). There are also other technical uses requiring detailed knowledge of mentioned above phenomena just to mention refrigeration installation with carbon dioxide as working fluid or supercritical pressurized water cooled reactors. In such applications either new fluids are considered or the conditions close to the thermodynamic critical point are exercised. Determination of pressure drop and heat transfer under such conditions is generally accomplished using dedicated empirical methods for specific fluids. It should be noticed however that in many cases the calculation methods are used for the conditions outside of the envelope of validity of predictive methods. Moreover, the considered calculation methods are usually developed for a restricted number of fluids and sometimes are used for other fluids claiming an incidental consistency.

When temperatures approach a thermodynamic critical point the surface tension and heat of vaporization decrease to reach a value of zero at the point. The intense nucleation process leads to high nucleate boiling heat transfer coefficients and at higher reduced pressures more pronounced dominance of nucleate boiling over convective boiling is seen [1–6].

The most extensively studied in literature working fluid under moderate and high reduced pressures was carbon dioxide [7–16] due to its potential air-conditioning and cooling applications. Literature concerning high values of reduced pressure for other fluids such as for example low boiling point refrigerants is still scarce. Additionally, most of the works focusing on high reduced pressures for low boiling point refrigerants were conducted for HFC refrigerants (R134a, R245fa, R22, R125, or mixtures of these) in conventional size channels [1,2,4,5,17]. Apart from the fact that HFC refrigerants are going to be replaced in the near future, most of the above-mentioned fluids have a critical temperature lower or equal to 100℃, except for R245fa (critical temperature equal to 154℃). Our study presents the results for R1233zd(E) (refrigerant from the HFO group) for saturation temperatures in the range from 115 to 145℃.

As mentioned earlier forthcoming applications in Organic Rankine Cycle systems and high-temperature heat pumps require more detailed knowledge on pressure drop and heat transfer. Operating temperatures of Organic Rankine Cycles are in the range from 50 to 150 °C [18] and there is a gap of knowledge in this area from the point of view of application of best potential working fluids. Desideri et al. [19] studied

---

Nomenclature

C_p	specific heat, [J/(kgK)]	δ	uncertainty, [%]
d	tube diameter, [m]	λ	thermal conductivity, [W/(mK)]
E	energy dissipation, [W/m³]	ρ	density, [kg/m³]
f	friction factor,	ɕ	surface tension, [N/m]
G	mass velocity, [kg/(m²s)]		
g	gravitational acceleration, [m/s²]	*Subscripts*	
HFC	hydrofluorocarbons	h	hydraulic
HFO	hydrofluoroolefins	in	inner
$\dot{m}$	mass flow, [kg/s]	LO	liquid state only
MAPE	mean absolute percentage error, [%]	MS	Müller-Steinhagen-Heck
p	pressure, [Pa]	out	outer
$\dot{q}$	heat flux, [W/m²]	Pb	pool boiling
$\dot{q}_v$	volumetric heat generation, [W/m²]	ph	preheater
r	radius, [m]	r	reduced conditions
T	temperature [K]	sat	saturation
x	vapor quality, [-]	ss	stainless steel
		sub	subcooled
Greek symbols		test	test section
α	heat transfer coefficient, [W/(m²K)]	TP	convective boiling
		TPB	total two-phase boiling
		VO	vapor state only

heat transfer and pressure drop of R245fa and R1233zd for saturation temperatures ranging from 100 to 130 °C, mass velocities from 62 to 102 kg/m²s, and heat fluxes from 9 to 37 kW/m². Contrary to the other studies, they found weak sensitivity of working fluids to the influence of both the saturation temperature and mass flux, which suggests that nucleate boiling is not the dominant heat transfer mechanism in the analyzed configuration.

Flow pattern determination is another important subject concerning two-phase flows. Understanding the interactions between vapor and liquid phases is a fundamental issue of two-phase flows. Flow pattern determination can be divided into two types of measurements: contact measurements and non-contact measurements. Regarding contact type measurements, Canière et al. [20] used a self-made capacitive void fraction sensor to study-two-phase flow patterns in macroscale tubes. Olivier et al. [21] analyzed fluctuations in the pressure drop gradients during the transition from intermittent to annular flow. Optical methods used to determine flow patterns are more common than contact ones. Revellin and Thome [22] developed the laser-based method which analyzed the frequency, coalescence rates, and length of bubbles exiting a microevaporator to distinguish the flow pattern maps. Ong and Thome [23] proposed an image processing method to determine the flow pattern transitions based on liquid film thickness on the top and bottom of the channel. These methods allow for the quantitative identification of two-phase flow patterns. Many studies are based on the objective investigation of the recorded images. Yang et al. [24] recorded images, with the use of a high-speed camera, of flow patterns during flow boiling of R600a in a 6 mm horizontal smooth tube. They identified four main flow regimes: plug flow, stratified-wavy flow, slug flow, and annular flow. They also noted that the transition between intermittent and annular flow was strongly influenced by mass velocity and heat flux. The higher the heat flux and mass flux, the lower the vapor quality of transition. Charnay et al. [25] used a high-speed camera to characterize the flow patterns of R245fa flow boiling. The tests were carried out in a 3 mm horizontal tube. In addition to image collecting the researchers analyzed the bubble frequency, the percentage of small bubbles, and the velocity of these bubbles. The authors highlighted that heat transfer is strongly related to the flow patterns, and that transitions between intermittent and annular flow overlap with the nucleate and convective boiling boundaries. The collected data showed the relation between heat flux and the transition from intermittent to annular flow. Liu et al. [26] studied the flow pattern characteristics of R245fa in a transparent

heated tube. Based on the images they determined six flow patterns: plug flow, stratified-wavy flow, intermittent flow, wavy-annular flow, and dryout/partial dryout flow. They observed that with the increase in mass velocity and heat flux, the transition from intermittent flow to annular flow moves to lower vapor qualities.

In the paper experiments are presented for the flow boiling of R1233zd(E) in a vertical tube aiming to extend the available experimental database. The flow visualization is also presented here inclusive of the flow maps. The presented study focuses on the identification of the influences of reduced pressure on heat transfer and pressure drop phenomena for a broad range of reduced pressures. The two-phase flow structures have also been identified for the collected experimental data. Additionally, the collected data enabled us to further validate the in-house model and to implement the effect of reduced pressure resulting in the new enhanced version of the model.

2. Experimental setup

The experiment has been conducted to measure the pressure drop and heat transfer characteristics of R1233zd(E) in flow boiling in a vertical stainless steel tube with an inside diameter of 3 mm and 1 mm wall thickness. The test section is 300 mm long. Earlier, a similar experiment was accomplished in the lab for a diameter of 2 mm [3]. The data collected for the former experiments were collected for the values of reduced pressures ranging from 0.2 to 0.7. Such data enabled analysis of the effect of reduced pressure on pressure drop and heat transfer. In the present experiment, the heat flux and mass velocities were fixed, with values of 20 kW/m² and 800 kg/m²s, respectively. The present experiment's novelty is the possibility of visualizing the flow boiling data in a transparent tube of the same inlet diameter as the test section. Table 1 presents the thermophysical properties of R1233zd(E)

Table 1
Properties of R1233zd(E) at different reduced pressures used in experiment.

Reduced pressure [-]	Saturation temperature [C]	Pressure [bar]	Liquid specific heat [kJ/kg]	Heat of vaporization [kJ/kg]
0.4	115.07	14.28	1.49	128.55
0.5	126.48	17.85	1.58	116.15
0.6	136.27	21.43	1.72	103.59
0.7	144.85	24.99	1.94	90.25

refrigerant for saturation temperatures considered in the tests, which were extracted from the EES database [27].

Fig. 1 presents a schematic diagram of the experimental facility. R1233zd(E) is circulated in the test loop by means of the gear pump. The mass flow rate is controlled either by the control of the rotational velocity of the pump, by the by-pass microvalve, or by the microvalve placed before the preheater. The Coriolis-type flowmeter Mass 2100 type DL3, characterized by 0.05 % measuring deviation, is used to measure the mass flow rate. The microvalve placed before the preheater is used to minimize the pressure effects during boiling phenomena. The microvalve opening is selected in a way that the pressure drop on the valve is much higher than the pressure drop due to the boiling process. In the 3000 mm long, spirally-shaped preheater, the refrigerant is initially heated and sometimes evaporated to achieve the demanded experimental conditions for the test section. Vapor quality at the inlet to the test section is controlled thanks to the preheater and enthalpy-based energy balance. Both the preheater and the test section are heated by the Joule effect using two different DC voltage suppliers. To maintain a stable pressure in the system a bladder accumulator Meak 1.4 is used, which is filled with liquid refrigerant on one side and nitrogen on the other one.

As mentioned earlier the test section consists of a 300 mm long stainless steel tube with an inside diameter of 3 mm as well as a 200 mm long borosilicate glass tube with the same inside diameter. Both sections are separated by the PEEK insulators, used to electrically separate the test section from the rest of the experimental facility. Two pressure transducers Vegabar 83 (with a 0–40 bar measuring range) and two K-type thermocouples are installed at the inlet and outlet of the test section. Additionally, pressure connectors are linked to the Vegadif 85 differential pressure transducer with a maximum of 50 kPa. Eighteen K-type thermocouples are soldered to the wall of the test section (nine pairs of thermocouples soldered at opposite sides of the tube at respective axial locations). The details of the test section are presented in Fig. 1.

The thermocouples were calibrated at 3 different temperature points at a certified laboratory which resulted in a significant uncertainty decrease. A precise scheme of the test section is presented in Fig. 1. Imaging data is collected with the use of a high-speed camera FASTCAM Mini UX100 which is used to observe flow structures in a non-opaque glass tube. Data acquisition is made with the use of National

Instruments NI PXIe-1071 (DAQ) connected to a PC. National Instruments LabView software is used for this purpose with in-house code.

3. Data processing and reduction

The heat transfer coefficient of R1233zd(E) is measured during the experiment. Presented below is a procedure for determination of the measurement uncertainties.

The root-sum-square (RSS) method [28] is used for error propagation, which reads:

$$\delta q = \sqrt{\left(\frac{\partial q}{\partial x}\delta x\right)^2 + .. + \left(\frac{\partial q}{\partial z}\delta z\right)^2} \tag{1}$$

where q is the experimental result calculated based on other variables (x, …, z) which are measured with a known uncertainty δ. Table 2 presents the sum up of experimental details with maximum values of calculated uncertainty. The uncertainty of the heat transfer coefficient determination varied from 13 % to 25 %.

Tests are carried out by monitoring the mass flux and calculating values of vapor quality and saturation temperature. Data is recorded when certain conditions are satisfied in a period of time of 10 min, namely the deviation of mass flux lower than 1.5 % of current value, the deviation of saturation temperature not higher than 0.5 K, and vapor quality deviation not higher than 1 %.

Enthalpy at the inlet of test section is calculated from the energy balance of the preheater:

$$h_1 = h_0 + \frac{\dot{Q}_{ph}}{\dot{m}} \tag{2}$$

where: h_0 is enthalpy at the inlet of the preheater, which is deduced from temperature and pressure measurements, Q_{ph} is the heat delivered to the fluid in the preheater, and $\dot{m}$ is the mass flow rate.

The vapor quality at a position y of the test section is calculated based on the local enthalpy calculations:

$$x_y = \frac{h_1 + \frac{\dot{Q}_{test}}{\dot{m}}\frac{l_y}{l_{test}} - h_{1.sat}}{h_{lv}} \tag{3}$$

where: x_y is vapor quality at the position y of the test section, $\dot{Q}_{test}$ is the heat delivered to the fluid in the test section, l_y is the position of the measurement point and l_{test} is the length of the test section, $h_{1.sat}$ is the saturated liquid enthalpy calculated for the saturation temperature, and h_{lv} is the latent heat of vaporization calculated for saturation temperature.

The fluid could enter the test section as either subcooled liquid or as a two-phase mixture. The further procedures are different depending on which case occurs during the experiment.

If the subcooled liquid enters the heat transfer test section the liquid pressure drop for the subcooled liquid region has to be calculated first.

$$\Delta P_l = \frac{2 \bullet G^2 \bullet f_l \bullet l_{sub}}{\rho_l \bullet d_{in}} \tag{4}$$
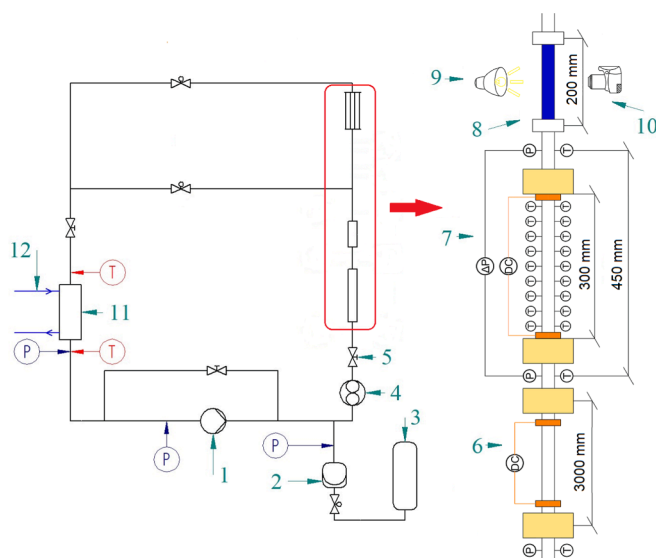

Fig. 1. Experimental facility schematic: 1 – diaphragm pump, 2 – bladder hydro-accumulator, 3 – pressurized nitrogen tank, 4 – Coriolis flowmeter, 5 – control valve, 6 – preheater, 7 – heat transfer test section, 8 – visualization test section, 9 – LED light source, 10 – fast camera, 11 – condenser, 12 – oil loop.

Table 2
Range of the experimental parameters in the study.

Parameters	Values	Uncertainty range
d (mm)	3.0	± 0.05
l (mm)	300	± 0.1
G (kg/m²s)	800	± 3.4 %
$\dot{q}$ preheater (kW/m²)	0.1 – 50.0	± 1.80 – 1.93 %
$\dot{q}$ test section (kW/m²)	20.0	± 4.3 %
T_{sat} (C)	115.1 – 144.85	± 0.34 – 0.41
P_{sat} (kPa):	1428–2499	± 14.0
x (-)	0.01 – 0.99	± 0.0041 – 0.0095
HTC (kW/(m²K))	5.98–24.66	± 13.44 – 25.18 %

where G denotes a mass velocity, l_{sub} is the subcooled length, f_l is friction factor calculated based on the Blasius correlation, ρ_l is a single phase density and d_{in} is the inside diameter of the test section.

The length of the tube which is occupied by subcooled liquid is deduced from the energy balance:

$$l_{sub} = \frac{\dot{m} \bullet c_p}{\dot{q}_{test} \bullet \pi \bullet d_{in}} \bullet (T_{sat} - T_1) \tag{5}$$

where q_{test} is a heat flux generated in the tube by the Joule effect.

Saturation temperature is deduced with the use of EES software on the basis of saturation pressure:

$$p_{sat.test} = p_{1.test} - \Delta p_l \tag{6}$$

Taking into account the saturation pressure from Eq. (6) the saturation temperature at position y for the first experimental case is calculated using thermal properties in EES:

$$T_{sat.y} = T_{sat}(p_{sat.y}) \tag{7}$$

where saturation pressure is calculated from the following equation:

$$p_{sat.y} = p_{sat.test} - (\Delta p_{total} - \Delta p_l) \bullet \left(\frac{l_y - l_{sub}}{l_{test} - l_{sub}}\right) \tag{8}$$

In the second experimental case, where saturated two-phase fluid enters the test section, the saturation pressure is calculated based on the following equation:

$$p_{sat.y} = p_{sat.test.in} - (\Delta p_{total}) \bullet \left(\frac{l_y}{l_{test}}\right) \tag{9}$$

The temperature at the inner wall at position y is deduced from Eq. (10) which was derived based on the assumption of uniform heat generation in the channel.

$$T_{wall.in.y} = T_{wall.out.y} + \frac{\dot{q}_V(r_{out}^2 - r_{in}^2)}{4 \bullet \lambda_{SS}} - \frac{\dot{q}_V \bullet r_{out}^2}{2 \bullet \lambda_{SS}} \bullet \ln\left(\frac{r_{out}}{r_{in}}\right) \tag{10}$$

where $T_{wall.out.y}$ is the temperature measured at position y, q_v is the volumetric heat generation, r_{out} is the radius of the outer wall, r_{in} is the radius of the inside wall and λ_{SS} is heat conductivity of the tube wall. The outer wall temperature is measured by two different thermocouples located on the opposite sides of the tube, that is why the average from both these thermocouples is taken into account:

$$T_{wall.in.y} = \frac{T_{wall.in.y1} + T_{wall.in.y2}}{2} \tag{11}$$

Finally the heat transfer coefficient at position y is calculated with Eq. (12):

$$\alpha_y = \frac{\dot{q}_{test}}{T_{wall.in.y} - T_{sat.y}} \tag{12}$$

4. Flow boiling heat transfer model

For the sake of modelling the effect of reduced pressure has been implemented in the in-house model [29,30]. The model is developed on the grounds of the hypothesis that energy dissipation in flow boiling constitutes of two influences namely, the energy dissipation from the nucleation process, E_{Pb}, and energy dissipation from the convective part of the flow, E_{TP}.

$$E_{TPB} = E_{TP} + E_{Pb} \tag{13}$$

The details of the model can be found in [29,30] and here only the final form of the model is presented in the form:

$$\frac{\alpha_{TPB}}{\alpha_{LO}} = \sqrt{R^n + \frac{1}{1+P}\left(\frac{\alpha_{Pb}}{\alpha_{LO}}\right)^2} \tag{14}$$

Term α_{LO} is the heat transfer coefficient calculated assuming that only liquid flows through the analyzed channel. Its value is determined with the use of the Dittus-Boelter correlation [31] for a turbulent flow, and with the equation Nu = 4.36 for the laminar flow. Exponent n in Eq. (14) is equal to 0.76 [29,30]. The two-phase flow multiplier R in Eq. (14) is a modified version of the Müller-Steinhagen'a and Heck correlation [32]. In the form used in the present paper it has been extended and validated for use at a whole range of reduced pressures [33]:

$$R_{MS} = \left[1 + 2\left(\frac{1}{f_1} - 1\right)x Con^m\right](1-x)^{\frac{1}{3}} + x^3\frac{1}{f_{1z}} \tag{15}$$

Exponent m takes -0.875 for minichannels and 0 for conventional channels. The criterion used to distinguish between mini- and macrochannels is a confinement number proposed by Kew and Cornwell [34], which states that for Con greater than 0.5 we deal with minichannels:

$$Con = \frac{\sqrt{\frac{\sigma}{g(\rho_l - \rho_v)}}}{d_h} \tag{16}$$

The functions f_1 and f_{1z} present the ratio of pressure drop in liquid flow to pressure drop in gas flow and a ratio of heat transfer coefficient in liquid flow to the heat transfer coefficient in gas flow respectively and are calculated using Eqs. (17) and (18):

$$f_1 = \frac{\left(\frac{dp}{dL}\right)_{LO}}{\left(\frac{dp}{dL}\right)_{VO}} \tag{17}$$

$$f_{1z} = \frac{\alpha_{LO}}{\alpha_{VO}} \tag{18}$$

Correction P has been also revisited in the present study. The effect of reduced pressure on the in-house model performance has been more precisely modelled through the influence of applied wall heat flux. That influence is considered in the model [29,30] by the presence of the boiling number Bo. Originally the exponent at that number was featuring a constant value. In the present study the exponent at the boiling number Bo has been modified to become a function of the reduced pressure p_r. Following the sensitivity analysis the parameter A present in (19) was assigned a fixed value of 3. The correction to the in-house model, which incorporates the effect of reduced pressure now yields:

$$P = 2,53 \bullet 10^{-3} Re_{LO}^{1,17} Bo^{Ap_r}(R_{MS} - 1)^{-0,65} \tag{19}$$

The pool boiling heat transfer coefficient α_{Pb} in Eq. (14) is calculated using the Cooper correlation for pool boiling [35]. That correlation has an internal dependence on the values of reduced pressure.

One should also notice the fact that the approach to obtain a solution in a complex flow based on summation of dissipation energy proved also to be successful in other cases. The approach using the concept of dissipation energy summation model has been earlier used by Mikielewicz to the two-phase bubbly flow in the boundary layer [36] or in modelling of the supercritical heat transfer [37]. Also in these cases consistent results have been obtained, which confirm the capability of the presented modelling to predict complex flows with heat transfer and non-linear effects. Energy based methods are alternative to traditional modelling approaches, producing reliable results. That is appreciated in numerous engineering applications, see for example Galerkin and other energy-based methods in mechanics.

5. Validation of experimental data

The correctness of experimental data has been first validated by performing single-phase tests. Based on the energy balance the preheater heat losses were estimated to be around 8 % of the heat lost to surroundings, whereas the test section losses were estimated at approximately 7 % of supplied heat. The obtained heat losses have been included in the estimation of experimental heat flux. The pressure drop results for a single-phase flow were compared with the Blasius

correlation [38]. Single-phase flow results for the heat transfer coefficient were compared with the models by Gnielinski [39] and Dittus-Boelter [31]. The results of the validation are presented in Figs. 2 and 3, respectively. The experimental data have been predicted with a mean absolute percentage error of 5.68 and 9.08 %, for Gnielinski and Dittus-Boelter respectively. The pressure drop was predicted with 5.09 % accuracy by the Blasius model. Such consistency of the results were found satisfactory and allowed for the accomplishment of the two-phase flow tests.

6. Experimental results

The experiment has been conducted for saturation temperatures ranging from 115 to 145 °C which corresponds to values of reduced pressures from 0.4 to 0.7. The mass velocity was equal to 800 kg/m²s and the heat flux was equal to 20 kW/m². Flow structures were constantly monitored in the transparent visualization test section with an inside diameter of 3 mm.

Figs. 4 and 5 present experimental results of the heat transfer coefficient and pressure drop in the function of vapor quality, for various values of reduced pressures. In the figures introduced also has been a line of transition between different flow structures encountered in the flow. The first dotted line represents the boundary between intermittent flow and churn flow and the second line represents a transition between wavy-annular and smooth-annular flow. Figs. 6-8 present images of various flow patterns for different values of reduced pressure and different values of vapor qualities. For vapor quality smaller than 0.5 the heat transfer coefficient increases with an increase in reduced pressure. Bubble generation intensifies with an increase in reduced pressure, which can for example be observed for vapor quality $x = 0.077$ in Figs. 7-8. Such a behaviour explains the intensification of heat transfer at the beginning of the evaporation process. The effect decreases with vapor quality and the heat transfer curves merge for vapor quality around 0.5. The effect corresponds to the creation of smooth-annular flow. Reduced pressure has also a significant impact on dryout phenomena. The dryout occurs earlier for higher values of reduced pressure. The pressure drop increases with a decrease in the value of reduced pressure. When the operating pressure approaches the thermodynamic critical point the density of liquid and vapor phases tends to the same value, and thus the velocity difference between phases decreases.
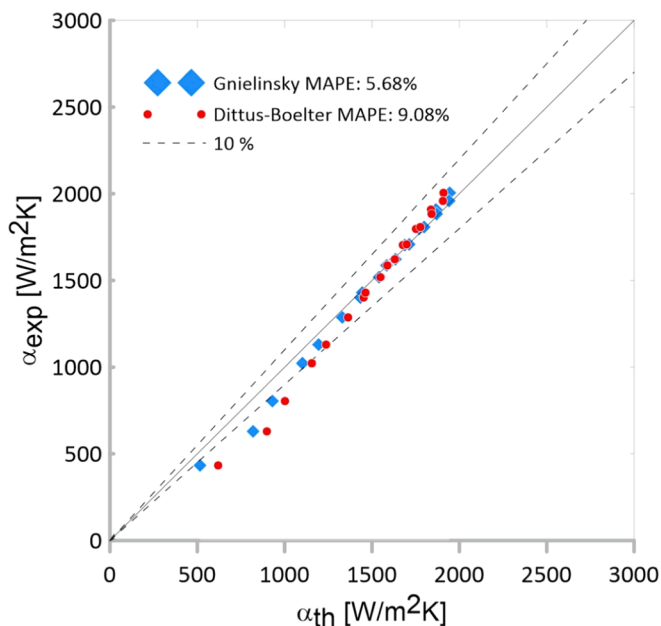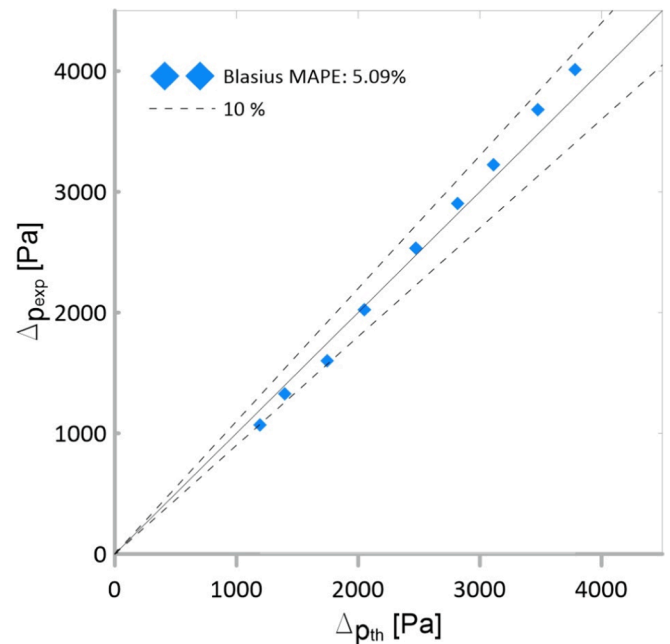

Fig. 3. Comparison of the experimental single-phase pressure drop with values obtained due to Blasius [38].
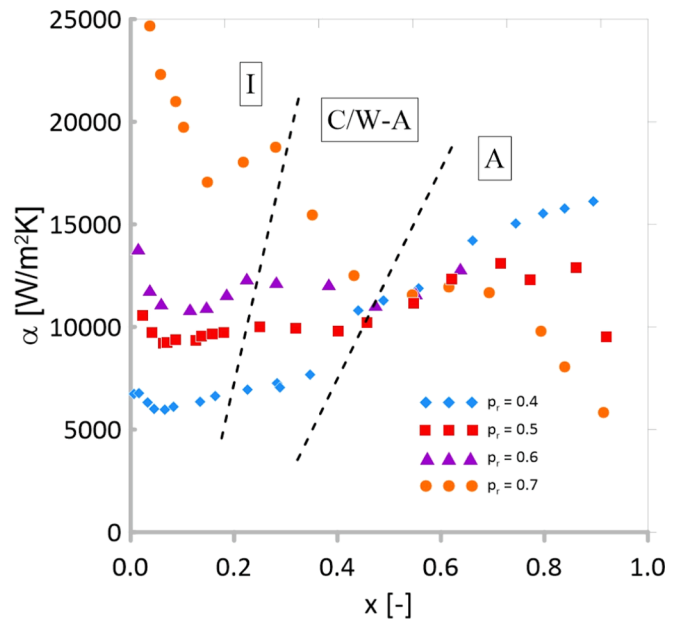

Fig. 4. Heat transfer coefficient as a function of vapor quality for different reduced pressures, heat flux q = 20 kW/m², and mass velocity G = 800 kg/m²s (I – intermittent flow; C/W-A – churn or wavy-annular flow; A – annular flow).

Moreover, the liquid surface tension also declines with reduced pressure rise which decreases the capillary forces. All of the mentioned phenomena lead to a diminution of pressure drop. The pressure drop also increases with the increase in vapor quality, which is associated with the increase of flow velocity due to the growth of two-phase specific volume [18]. These results confirm the findings of other authors [1,5,40–43]. The slope of the increase is not constant. After the transition from intermittent flow to annular flow, it can be observed that the pressure drop trend change and then sharply increase for higher vapor qualities. The pressure drop increase rate is smaller in the area between the churn flow and fully annular flow, which is explained by a smaller friction
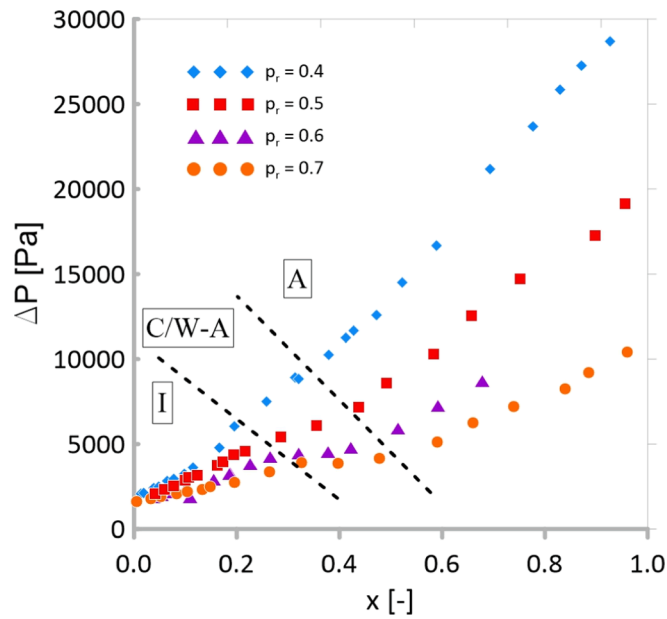

Fig. 2. Comparison of the single-phase test results α_{exp} with α_{th} obtained using the Gnielinski [39] and Dittus-Boelter [31] correlations.

Fig. 5. Pressure drop as a function of vapor quality for different reduced pressures, heat flux q = 20 kW/m^2, and mass velocity G = 800 kg/m^{2}s (I – intermittent flow; C/W-A – churn or wavy-annular flow; A – annular flow).
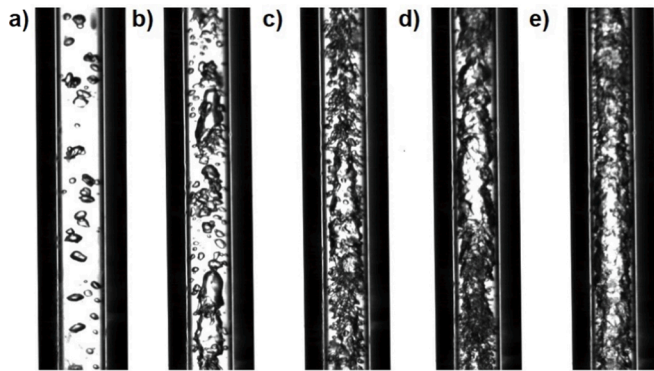

Fig. 6. Flow structures for reduced pressure pr = 0.4, heat flux q = 20 kW/m^2 and mass velocity G = 800 kg/m^{2}s: a) vapor quality x = 0.051; b) x = 0.113; c) x = 0.129; d) x = 0.165; e) x = 0.314.
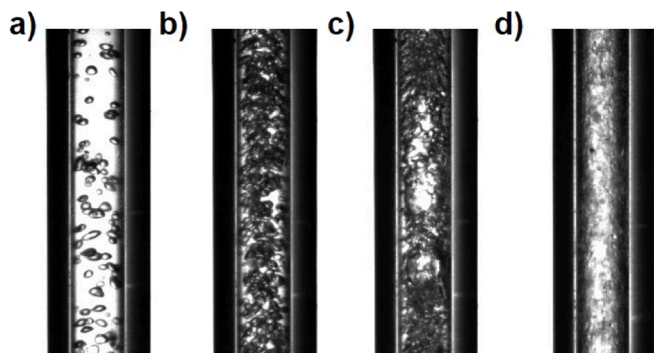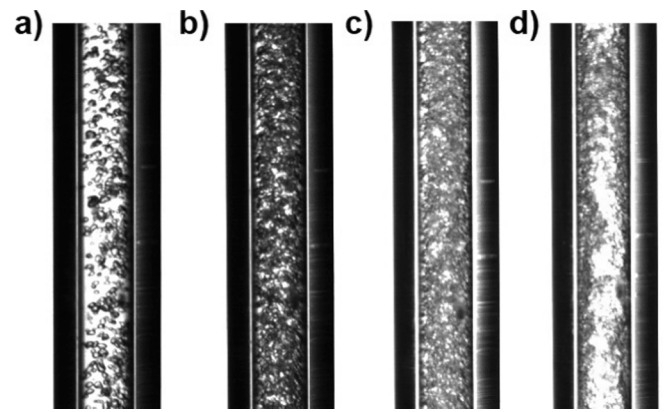

Fig. 7. Flow structures for reduced pressure p$_r$ = 0.5, heat flux q = 20 kW/m2 and mass velocity G = 800 kg/m^{2}s: a) vapor quality x = 0.077; b) x = 0.123; c) x = 0.173; d) x = 0.752.

factor for the smooth-annular flow than for the churn/wavy-annular flow.

The effect of vapor quality on heat transfer strongly depends on the

Fig. 8. Flow structures for reduced pressure p$_r$ = 0.6, heat flux q = 20 kW/m2 and mass velocity G = 800 kg/m^{2}s: a) vapor quality x = 0.077; b) x = 0.111; c) x = 0.226; d) x = 0.321.

value of reduced pressure. At the beginning of the evaporation process, the deterioration in heat transfer is observed. The latter can be explained by the dominance of nucleate boiling. A sudden increase in the number of bubbles in close proximity to the wall leads to a decrease in heat transfer capabilities. For the reduced pressure p$_r$ = 0.4 a characteristic rise in the heat transfer coefficient is observed as the vapor quality increases. The effect of nucleate boiling starts to diminish and it is taken over by convective boiling. Small growth can be also observed in the case of other curves, however, its effect weakens with the increase in reduced pressure value. The shape of obtained curves reassembles the letter "U", similarly as in the work by Marchetto et al. [18], where also "U" shaped heat transfer coefficient distributions have been detected. Nucleate boiling is the most dominant process for higher values of reduced pressure. A similar observation could be deduced from flow patterns presented in Figs. 6-8. The boundary from intermittent flow to annular flow shifts to higher values of vapor quality with an increase in reduced pressure.

7. Model validation

One of the main goals of this work was to implement the effect of reduced pressure in the in-house model and to validate it against the experimental database. The modeling database consists of data from the current study as well as data from the previous study [3], which was performed for a smaller channel diameter (2 mm) and reduced pressures ranging from 0.2 to 0.7. The data from previous work has been produced for mass velocities ranging from 400-1000 kg/m^{2}s, heat fluxes from 20 to 45 kW/m^2, and a entire range of vapor quality. Datapoints were also compared with an unmodified version of the model [4] as well as with four different correlations, which proved their usability in the work by Marchetto et al. [18], namely correlations due to Liu and Winterton [44], Kandlikar and Balasubramanian [45], Saitoh et al. [46] and Kanizawa et al. [47]. Finally, the in-house model has been tested against data obtained by Charnay et al. [17,48–50], which covers reduced pressures between 0.13 and 0.53. Only pre-dryout data has been analysed. The identification of dryout phenomena was related to the shape of the heat transfer trends. For most of the database, the occurrence of dryout was recognized by the sudden drop in heat transfer (an increase in the wall temperature). Whereas in the case of decreasing heat transfer trends, the dryout was associated with a 20 % or higher heat transfer coefficient drop across the vapor quality increment of 0.1.

The results of the comparison are presented in Figs. 9-20. Figs. 9, 11, 13, 15, 17, and 19 present a comparison between theoretical and experimental results with a 30 % error band. Of all six models, the enhanced version of the in-house model, i.e. with implemented corrected value of exponent at the boiling number Bo in eq. (19), shows the
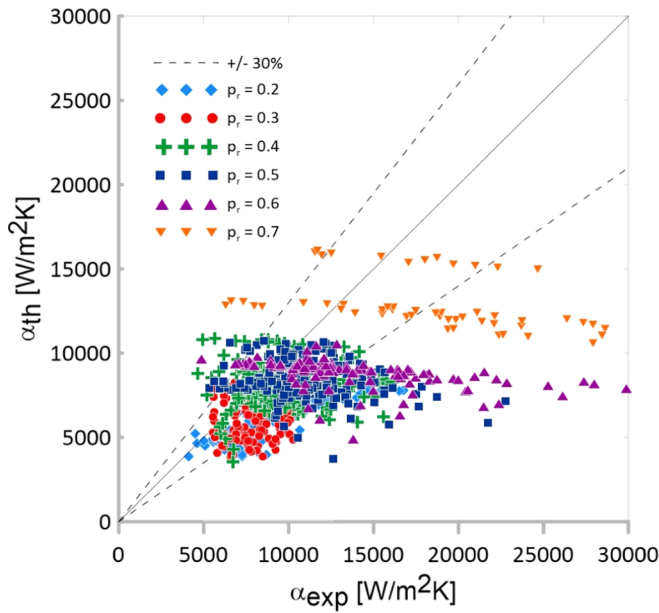
Fig. 9. Comparison between theoretical results achieved with the old version of the model with experimental data for R1233zd(E).
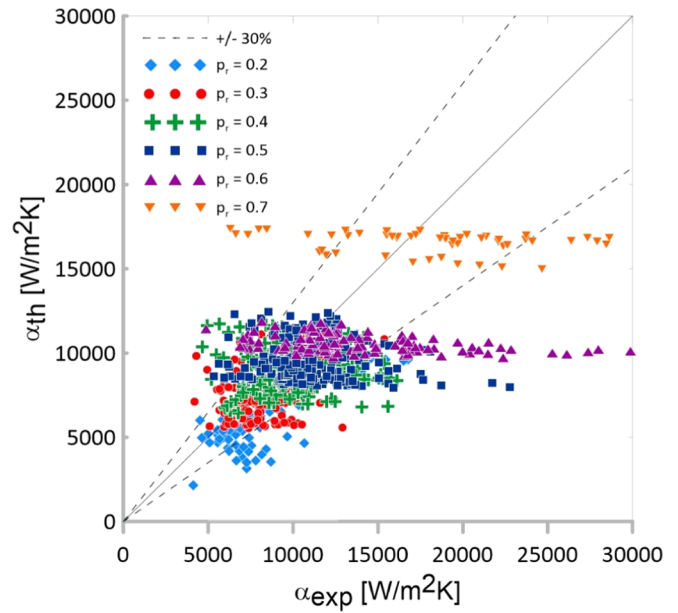

Fig. 11. Comparison between theoretical results achieved with a modified version of the model with experimental data for R1233zd(E).
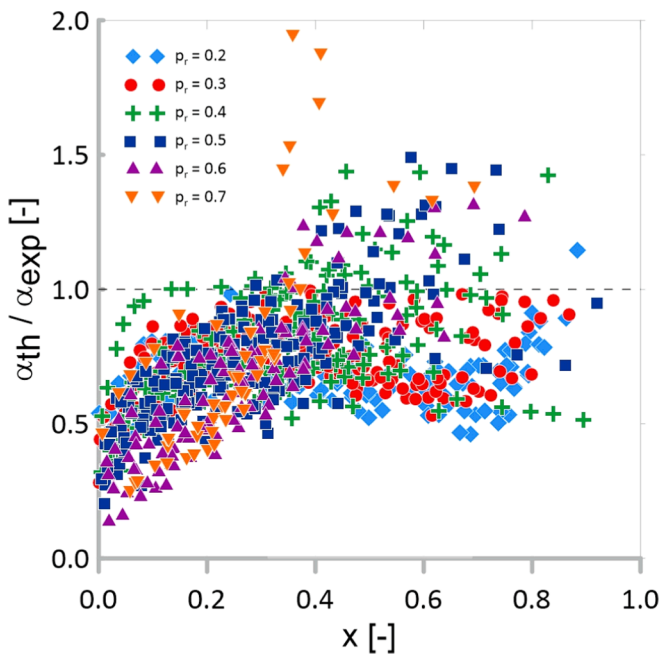

Fig. 10. Ratio between theoretical results (old version of the model) and experimental results in the function of vapor quality, x.
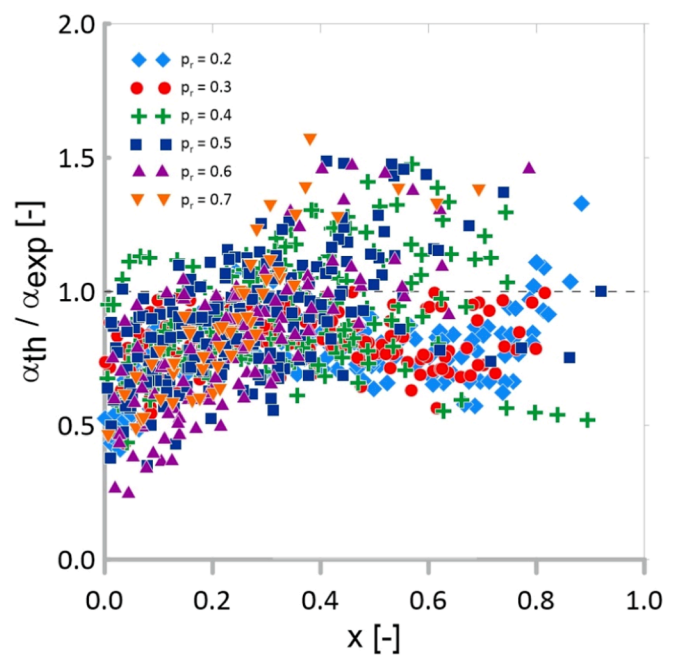

Fig. 12. Ratio between theoretical results (a modified version of the model) and experimental results in the function of vapor quality, x.

highest accuracy. The mean absolute percentage error (MAPE) for the whole database was equal to 23.17 % and 73.58 % of data fell within the 30 % error band. It is a significant increase compared to the previous version of the model which reached MAPE equal to 30.93 % and had 49.43 % of data within the 30 % error band range. Out of the all other considered correlations, only the one proposed by Kanizawa et al. [47] achieved similar accuracy with MAPE equal to 26.41 and 72.11 of datapoints within the 30 % error band. Results for all of the correlations are summed up in Table 3. Liu and Winterton's correlation predicted data with MAPE = 30.49 %, whereas Kandlikar and Balasubramanian correlation with MAPE = 33.24 %. Figs. 10, 12, 14, 16, 18, and 20 show the ratio of heat transfer coefficients between theoretical results and

experimental data in function of vapor quality. That type of graph allows us to interpret the results within the whole vapor quality range. The most noticeable improvement between the base and the enhanced model is seen in the region of low vapor quality value. In the previous version of the model, data in this region was strongly underestimated, whereas, in the new version of the model, the ratio tends to one. Figs. 21 and 22 show the results of each of the models across all investigated reduced pressures. The enhanced in-house model demonstrated the lowest MAPE for reduced pressures, $p_r = 0.2–0.5$, whereas for reduced pressures, $p_r = 0.6$ and 0.7 the correlation by Kanizawa [47] produced slightly better results. The model exceeded the 30 % error band only in the case of $p_r = 0.7$, which is caused by decreasing heat transfer trend presented for this
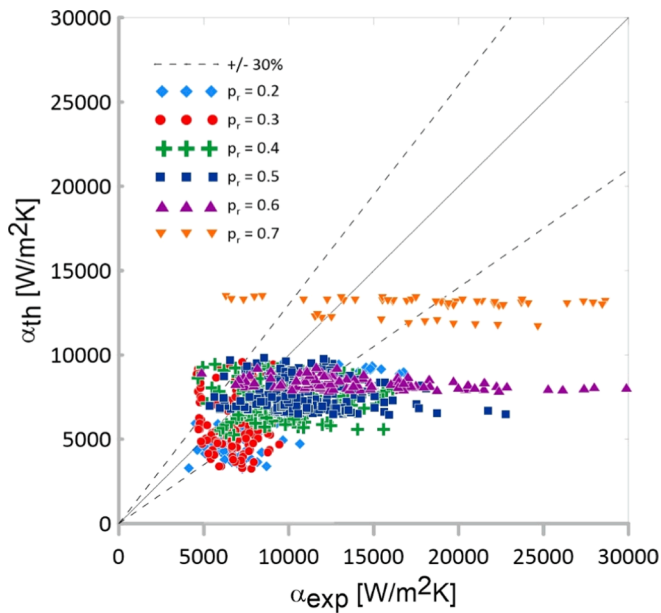
Fig. 13. Comparison between theoretical results achieved with Liu and Winterton correlation [44] with experimental data for R1233zd(E).
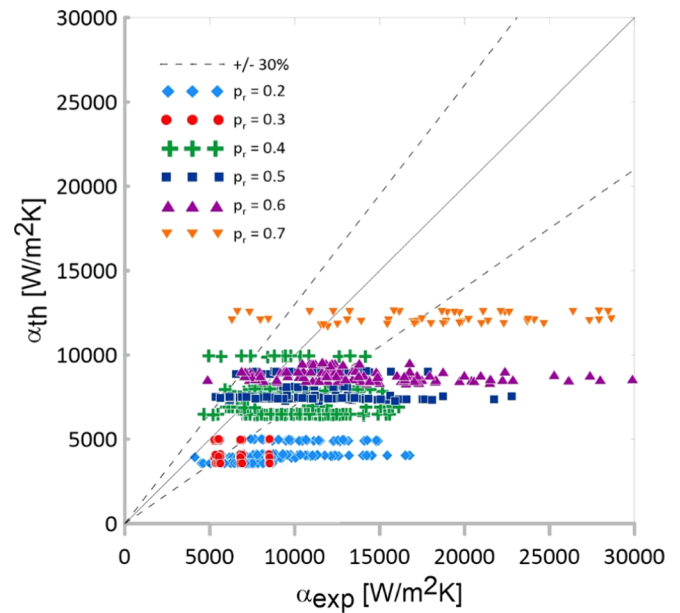

Fig. 15. Comparison between theoretical results achieved with correlation by Kandlikar and Balasubramanian [45] with experimental data for R1233zd(E).
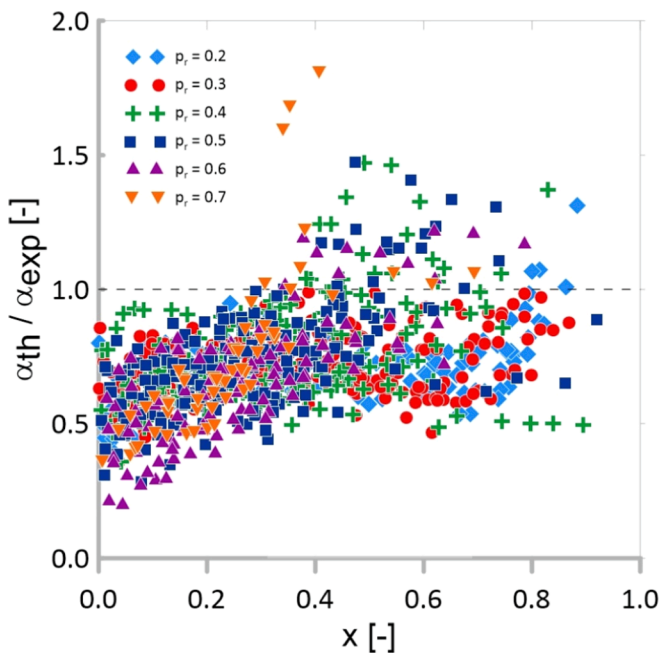

Fig. 14. Ratio between theoretical results (Liu and Winterton [44]) and experimental results in the function of vapor quality, x.
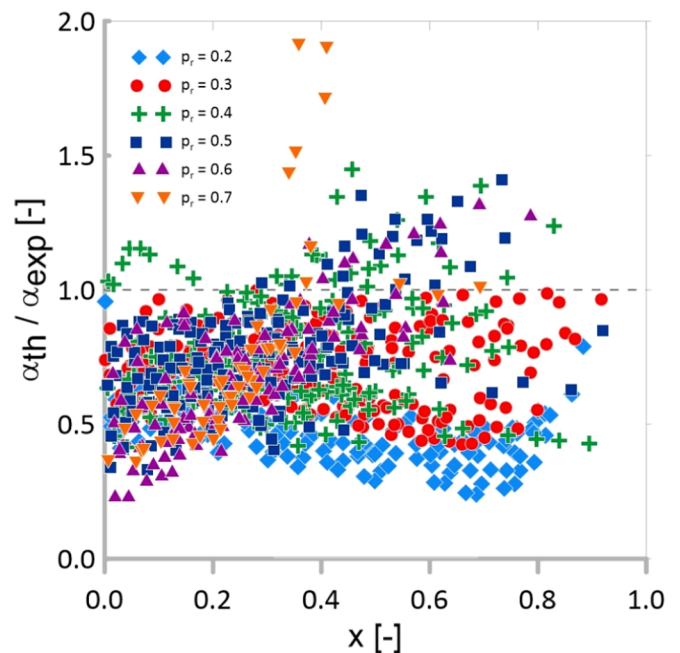

Fig. 16. Ratio between theoretical results (Kandlikar and Balasubramanian [45]) and experimental results in the function of vapor quality, x.

pressure. Generally, the model by Kanizawa estimated the highest share of datapoints within the 30 % error band and only in the case of reduced pressure, $p_r = 0.3$ failed to predict more than 50 % of data points. The latter can be explained by a small amount of data for this particular reduced pressure. Overall, the enhanced version of the model estimated a slightly bigger portion of data within the 30 % error band than the correlation by Kanizawa. A qualitative comparison between data and models is shown in Figs. 23 and 24. Despite its simplicity, the modified model reflects the thermodynamic trends with high accuracy.

The modified version of the in-house model has also been tested against the database collected for R245fa by Charnay et al. [17,48–50]. R1233zd(E) is considered a replacement for R245fa, due to the similar

thermophysical properties of both fluids. The results of the comparison are presented in Figs. 25 and 26. The mean absolute percentage error was equal to 19.23 % and 78.34 % of data fell within the 30 % error band. Such a result can be regarded as quite satisfactory, and better than the other heat transfer correlations tested by Charnay et al. [15–18].

8. Conclusions

Experimental data of heat transfer and pressure drop for R1233zd(E) in a 3 mm inside diameter tube, for different reduced pressures was presented. The authors discussed the effect of reduced pressure, flow structures, and vapor quality on heat transfer trends.
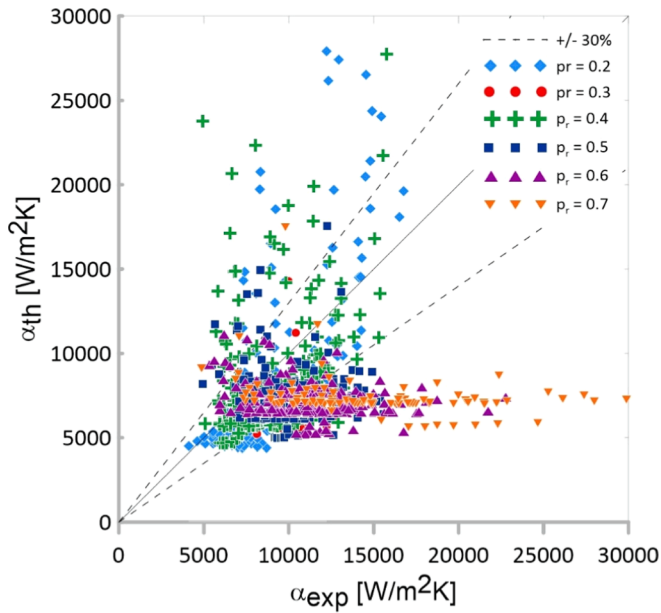
Fig. 17. Comparison between theoretical results achieved with correlation by Saitoh et al. [46] with experimental data for R1233zd(E).
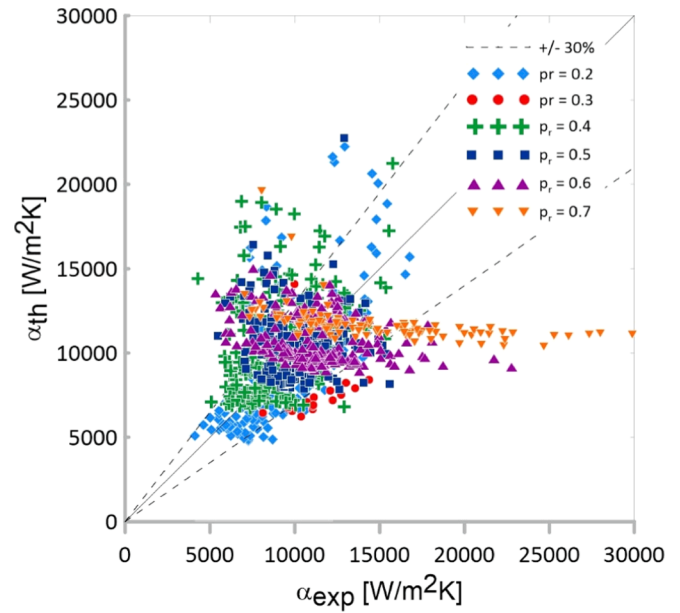

Fig. 19. Comparison between theoretical results achieved with correlation by Kanizawa et al. [47] with experimental data for R1233zd(E).
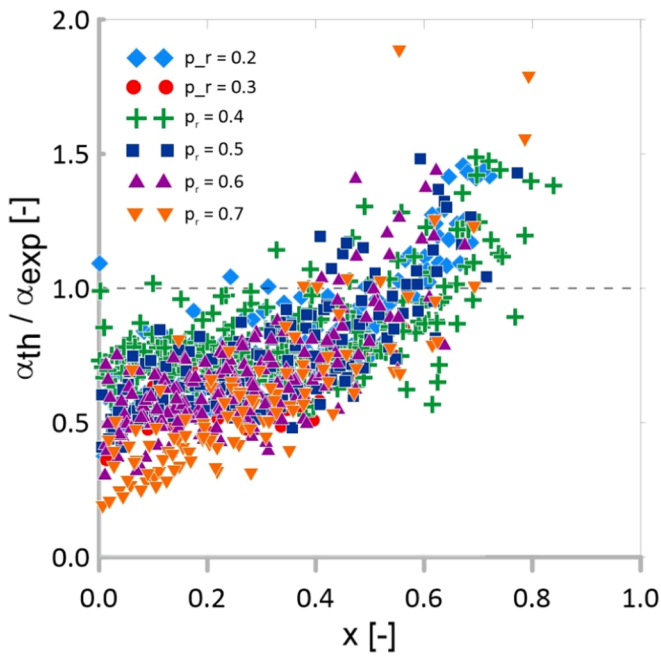

Fig. 18. Ratio between theoretical results (Saitoh et al. [46]) and experimental results in the function of vapor quality, x.
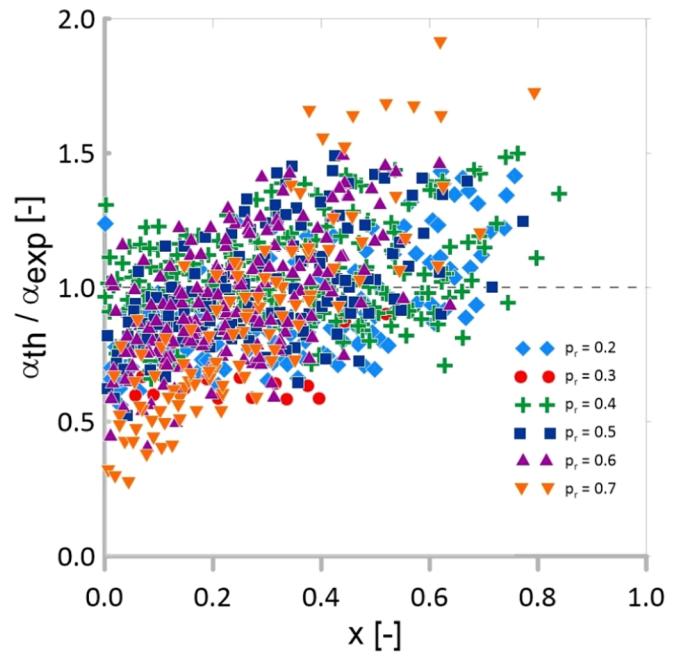

Fig. 20. Ratio between theoretical results (Kanizawa et al. [47]) and experimental results in the function of vapor quality, x.

The major conclusions from accomplished experiments are that the heat transfer coefficient increases and pressure drop decreases with the increase of reduced pressure. All of the obtained heat transfer trends initially decrease with vapor quality and then do not change or increase with vapor quality. The decrease is connected to the dominance of the nucleate boiling phenomena. The subsequent increase in heat transfer indicates the increased effect of convective boiling which corresponds to the transition from intermittent to churn flow. The rate of the increase depends on the value of reduced pressure (the smaller the reduced pressure the higher the rate). Around vapor quality equal to $x = 0.5$, the curves merge. The latter is related to the smoothing of the liquid film. The pressure drop curves increase with vapor quality and the rate of

Table 3
Results of comparison between the collected experimental data and selected flow boiling heat transfer correlations.

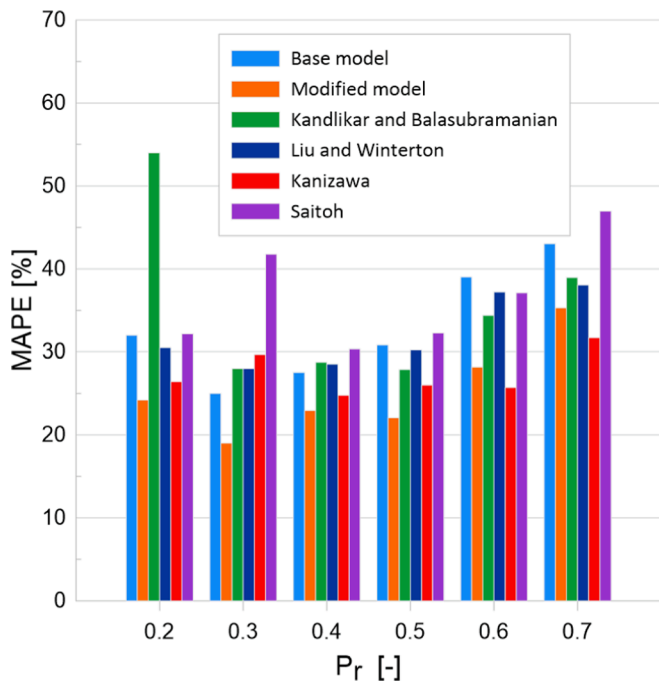|	Mean Absolute percentage error [%]	Fraction of data within 30 % error band [%]
Base model [29,30]	30.93	49.43
Modified model	23.17	73.58
Liu and Winterton [44]	30.49	49.56
Kandlikar and Balasubramanian [45]	33.24	43.32
Saitoh et al. [46]	34.75	46.63
Kanizawa et al. [47]	26.41	72.11

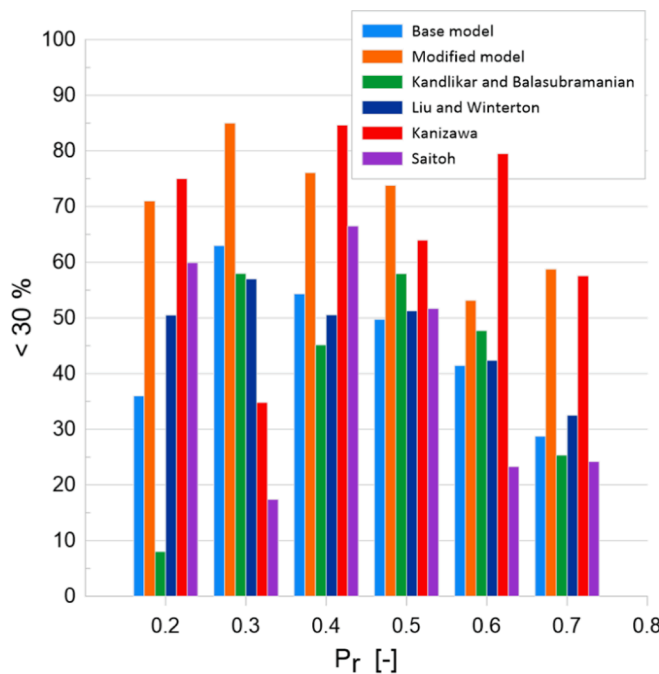**Fig. 21.** MAPE for all of the reduced pressures considered in a current and previous study [3].

Fig. 22. The amount of data within the 30% error band range for all of the reduced pressures considered in a current and previous study [3].

Fig. 23. Heat transfer coefficient as a function of vapor quality for reduced pressure $p_r = 0.5$, heat flux q = 20 kW/m^2, and mass velocity G = 800 kg/m^{2}s compared to models used in the work.

Fig. 24. Heat transfer coefficient as a function of vapor quality for reduced pressure $p_r = 0.2$, heat flux q = 20 kW/m^2, and mass velocity G = 600 kg/m^{2}s compared to models used in the work. Experimental data from the previous study [3].

growth depends on the value of reduced pressure. Additionally, pressure drop in considered reduced pressures is influenced by the type of annular flow (churn flow, wavy-annular, smooth-annular).

In the case of reduced pressure $p_r = 0.4$, both nucleate and convective boiling are present. For reduced pressures equal to or higher than 0.5 the nucleate boiling starts to be the dominant heat transfer mechanism. For these reduced pressures bubbles were observed in the flow within a broad range of vapor quality (e.g. x = 0.22 for reduced pressure equal to 0.6).
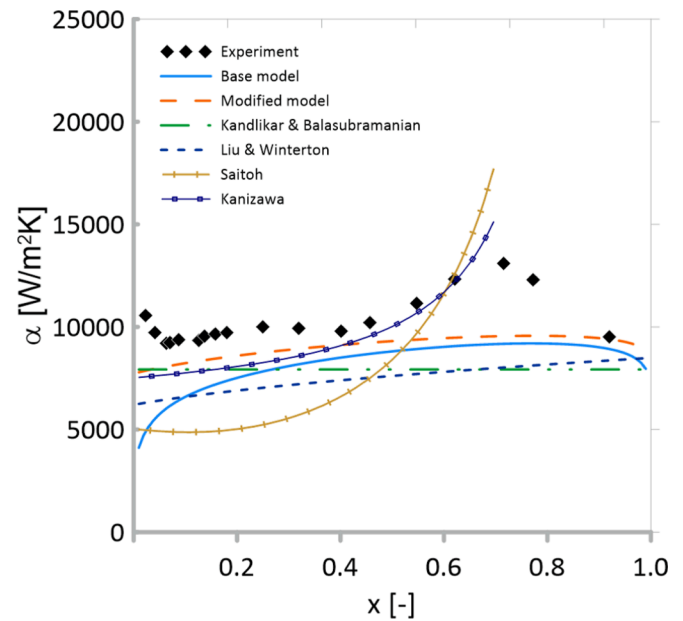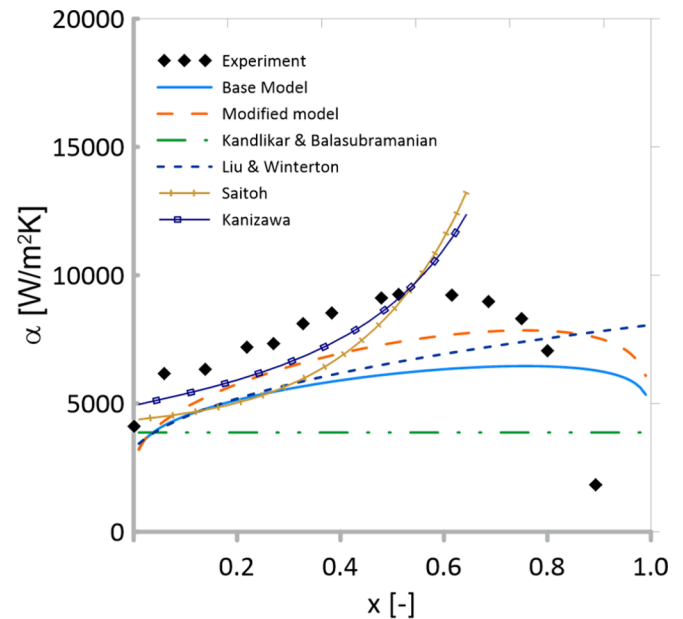
The heat transfer database for R1233zd(E) and R245fa has been compared with several predictive methods, namely the reference in-house model [29,30], modified in-house model, and correlations by Liu and Winterton [44], Kandlikar and Balasubramanian [45] Kanizawa et al. [47] and Saitoh et al. [46]. The modified version of the model showed the highest accuracy, with MAPE equal to 23.17 % for R1233zd (E) and 19.23 % for R245fa. The model has proven itself across various reduced pressures: 0.3–0.7 for R1233zd(E) and 0.13–0.53 for R245fa, which was the main goal of the conducted work. Of all other correlations used, the one by Kanizawa et al. estimated experimental data with the highest accuracy, resulting in MAPE 26.41 % and 72.11 % of datapoints
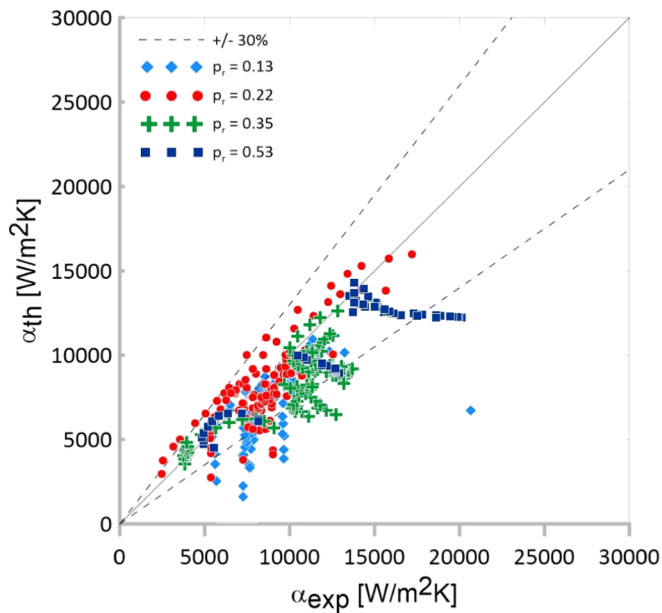
Fig. 25. Comparison between theoretical results achieved with an enhanced version of the model with experimental data for R245fa [17,48–50].
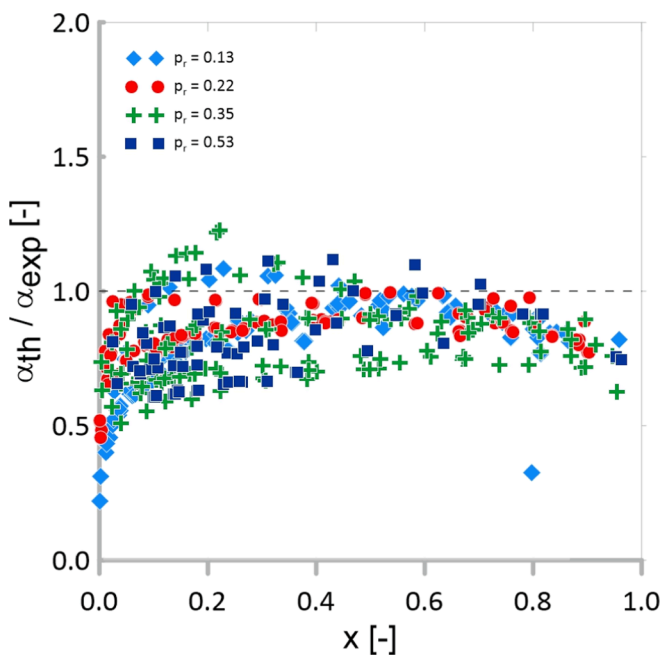

Fig. 26. Ratio between theoretical results (enhanced version of the model) and experimental results for R245fa [17,48–50] in the function of vapor quality, x.

predicted within the 30 % error band.

Declaration of Competing Interest

The authors declare that they have no known competing financial interests or personal relationships that could have appeared to influence the work reported in this paper.

Data availability

Data will be made available on request.

References

[1] G. Lillo, R. Mastrullo, A.W. Mauro, F. Pelella, L. Viscito, Experimental thermal and hydraulic characterization of R448A and comparison with R404A during flow boiling, Appl Therm Eng 161 (2019), 114146, https://doi.org/10.1016/j.applthermaleng.2019.114146.

[2] D. Del Col, Flow boiling of halogenated refrigerants at high saturation temperature in a horizontal smooth tube, Exp Therm Fluid Sci 34 (2) (2010) 234–245, https://doi.org/10.1016/j.expthermflusci.2009.10.035.

[3] M. Pysz, S. Głuch, D. Mikielewicz, Experimental study of flow boiling pressure drop and heat transfer of R1233zd(E) at moderate and high saturation temperatures, Int J Heat Mass Transf 204 (2023), 123855, https://doi.org/10.1016/j.ijheatmasstransfer.2023.123855.

[4] M. Billiet, B. Ameel, R. Charnay, R. Revellin, M. De Paepe, Flow regime based heat transfer correlation for R245fa in a 3 mm tube, Int J Heat Mass Transf 117 (2018) 1304–1311, https://doi.org/10.1016/j.ijheatmasstransfer.2017.10.062.

[5] S. Grauso, R. Mastrullo, A.W. Mauro, G.P. Vanoli, Two-phase adiabatic frictional pressure gradients for R410A and CO2 in a macro channel: Experiments and a simplified predictive method for annular flow from low to medium reduced pressures, Exp Therm Fluid Sci 52 (2014) 79–87, https://doi.org/10.1016/j.expthermflusci.2013.08.024.

[6] Y. Zhang, R. Tan, X. Dai, D. Wang, Y. Ma, H. Li, L. Shi, Experimental study of R134a flow boiling in a horizontal tube for evaporator design under typical Organic Rankine Cycle pressures, Int J Heat Fluid Flow 71 (2018) 210–219, https://doi.org/10.1016/j.ijheatfluidflow.2018.04.008.

[7] X. Lei, W. Zhang, J. Zhang, N. Dinh, H. Li, Experimental investigations on the boiling heat transfer of horizontal flow in the near-critical region, Int J Heat Mass Transf 125 (2018) 618–628, https://doi.org/10.1016/j.ijheatmasstransfer.2018.04.043.

[8] J. Pettersen, Flow vaporization of CO2 in microchannel tubes, Exp Therm Fluid Sci 28 (2–3) (2004) 111–121, https://doi.org/10.1016/S0894-1777(03)00029-3.

[9] T. Ami, N. Nakamura, H. Umekawa, M. Ozawa, and M. Shoji, "Flow Pattern and Boiling Heat Transfer of CO2 at High Pressure in Horizontal Mini-Channels," in *2010 14th International Heat Transfer Conference, Volume 1*, ASMEDC, Jan. 2010, pp. 307–316. 10.1115/IHTC14-22560.

[10] H. Zahlan, D. Groeneveld, S. Tavoularis, Measurements of convective heat transfer to vertical upward flows of CO2 in circular tubes at near-critical and supercritical pressures, Nucl. Eng. Des. 289 (2015) 92–107, https://doi.org/10.1016/j.nucengdes.2015.04.013.

[11] A. Eter, D. Groeneveld, S. Tavoularis, Convective heat transfer at high subcritical pressures in tubes with and without flow obstacles, Nucl. Eng. Des. 318 (2017) 1–23, https://doi.org/10.1016/j.nucengdes.2017.04.013.

[12] C. Dang, N. Haraguchi, T. Yamada, M. Li, E. Hihara, Effect of lubricating oil on flow boiling heat transfer of carbon dioxide, Int. J. Refrig 36 (1) (2013) 136–144, https://doi.org/10.1016/j.ijrefrig.2012.09.020.

[13] K.-I. Choi, M. Rifaldi, A. S. Pamitran, and J.-T. Oh, "Characteristics of Two-Phase Flow Boiling Heat Transfer and Pressure Drop of NH3, C3H8 and CO2 in Horizontal Circular Small Tubes," in *2010 14th International Heat Transfer Conference, Volume 1*, ASMEDC, Jan. 2010, pp. 407–413. 10.1115/IHTC14-22660.

[14] J.M. Cho, Y.J. Kim, M.S. Kim, Experimental studies on the evaporative heat transfer and pressure drop of CO2 and CO2/propane mixtures flowing upward in smooth and micro-fin tubes with outer diameter of 5 mm for an inclination angle of 45°, Int. J. Refrig 33 (5) (2010) 922–931, https://doi.org/10.1016/j.ijrefrig.2010.02.002.

[15] Y.J. Kim, J.M. Cho, M.S. Kim, Experimental study on the evaporative heat transfer and pressure drop of CO2 flowing upward in vertical smooth and micro-fin tubes with the diameter of 5 mm, Int. J. Refrig 31 (5) (2008) 771–779, https://doi.org/10.1016/j.ijrefrig.2007.12.001.

[16] J.M. Cho, M.S. Kim, Experimental studies on the evaporative heat transfer and pressure drop of CO2 in smooth and micro-fin tubes of the diameters of 5 and 9.52mm, Int. J. Refrig 30 (6) (2007) 986–994, https://doi.org/10.1016/j.ijrefrig.2007.01.007.

[17] R. Charnay, R. Revellin, J. Bonjour, Flow boiling heat transfer in minichannels at high saturation temperatures: Part I - Experimental investigation and analysis of the heat transfer mechanisms, Int J Heat Mass Transf 87 (2015) 636–652, https://doi.org/10.1016/j.ijheatmasstransfer.2015.03.081.

[18] D.B. Marchetto, D.C. Moreira, R. Revellin, G. Ribatski, A state-of-the-art review on flow boiling at high reduced pressures, Int J Heat Mass Transf 193 (2022), 122951, https://doi.org/10.1016/j.ijheatmasstransfer.2022.122951.

[19] A. Desideri, J. Zhang, M.R. Kærn, T.S. Ommen, J. Wronski, V. Lemort, F. Haglind, An experimental analysis of flow boiling and pressure drop in a brazed plate heat exchanger for organic Rankine cycle power systems, Int J Heat Mass Transf 113 (2017) 6–21, https://doi.org/10.1016/j.ijheatmasstransfer.2017.05.063.

[20] H. Canière, B. Bauwens, C. T'Joen, M. de Paepe, Mapping of horizontal refrigerant two-phase flow patterns based on clustering of capacitive sensor signals, Int J Heat Mass Transf 53 (23–24) (2010) 5298–5307, https://doi.org/10.1016/j.ijheatmasstransfer.2010.07.027.

[21] J.A. Olivier, L. Liebenberg, J.R. Thome, J.P. Meyer, Heat transfer, pressure drop, and flow pattern recognition during condensation inside smooth, helical micro-fin,

and herringbone tubes, Int. J. Refrig 30 (4) (2007) 609–623, https://doi.org/10.1016/j.ijrefrig.2006.11.003.

[22] R. Revellin, J.R. Thome, Experimental investigation of R-134a and R-245fa two-phase flow in microchannels for different flow conditions, Int J Heat Fluid Flow 28 (1) (2007) 63–71, https://doi.org/10.1016/j.ijheatfluidflow.2006.05.009.

[23] C.L. Ong, J.R. Thome, Macro-to-microchannel transition in two-phase flow: Part 1 – Two-phase flow patterns and film thickness measurements, Exp Therm Fluid Sci 35 (1) (2011) 37–47, https://doi.org/10.1016/j.expthermflusci.2010.08.004.

[24] Z. Yang, M. Gong, G. Chen, X. Zou, J. Shen, Two-phase flow patterns, heat transfer and pressure drop characteristics of R600a during flow boiling inside a horizontal tube, Appl Therm Eng 120 (2017) 654–671, https://doi.org/10.1016/j.applthermaleng.2017.03.124.

[25] R. Charnay, R. Revellin, J. Bonjour, Flow pattern characterization for R-245fa in minichannels: Optical measurement technique and experimental results, Int. J. Multiph. Flow 57 (2013) 169–181, https://doi.org/10.1016/j.ijmultiphaseflow.2013.05.015.

[26] J. Liu, J. Liu, X. Xu, Diabatic visualization study of R245fa two phase flow pattern characteristics in horizontal smooth and microfin tube, Int J Heat Mass Transf 152 (2020), 119513, https://doi.org/10.1016/j.ijheatmasstransfer.2020.119513.

[27] "European Social Survey European Research Infrastructure (ESS ERIC). (2022). ESS20 - integrated file, edition 1.2 . Sikt - Norwegian Agency for Shared Services in Education and Research. https://doi.org/10.21338/ESS10E01.".

[28] J. Taylor, Introduction to error analysis, the study of uncertainties in physical measurements. 1997.

[29] D. Mikielewicz, A New Method for Determination of Flow Boiling Heat Transfer Coefficient in Conventional-Diameter Channels and Minichannels, Heat Transfer Eng. 31 (4) (2010) 276–287, https://doi.org/10.1080/01457630903311694.

[30] D. Mikielewicz, J. Mikielewicz, J. Tesmar, Improved semi-empirical method for determination of heat transfer coefficient in flow boiling in conventional and small diameter tubes, Int J Heat Mass Transf 50 (19–20) (2007) 3949–3956, https://doi.org/10.1016/j.ijheatmasstransfer.2007.01.024.

[31] F.W. Dittus, L.M.K. Boelter, Heat transfer in automobile radiators of the tubular type, Int. Commun. Heat Mass Transfer 12 (1) (1985) 3–22.

[32] H. Müller-Steinhagen, K. Heck, A simple friction pressure drop correlation for two-phase flow in pipes, Chem. Eng. Process. 20 (6) (1986) 297–308, https://doi.org/10.1016/0255-2701(86)80008-3.

[33] D. Mikielewicz, J. Mikielewicz, An improved Müller-Steinhagen and Heck model for two phase pressure drop modelling at high reduced pressures, Journal of Power Technologies 102 (2022) 81–87.

[34] P.A. Kew, K. Cornwell, Correlations for the prediction of boiling heat transfer in small-diameter channels, Appl Therm Eng 17 (8–10) (1997) 705–715, https://doi.org/10.1016/S1359-4311(96)00071-3.

[35] M.G. Cooper, "Saturation nucleate pool boiling - a simple correlation", First U.K National Conference on Heat Transfer, Elsevier (1984) 785–793, https://doi.org/10.1016/B978-0-85295-175-0.50013-8.

[36] D. Mikielewicz, Hydrodynamics and heat transfer in bubbly flow in the turbulent boundary layer, Int J Heat Mass Transf 46 (2) (2003) 207–220, https://doi.org/10.1016/S0017-9310(02)00287-9.

[37] D. Mikielewicz, J. Mikielewicz, Modelling of heat transfer in supercritical pressure recuperators, Energy 207 (2020), 118251, https://doi.org/10.1016/j.energy.2020.118251.

[38] H. Blasius, "Das Aehnlichkeitsgesetz bei Reibungsvorgängen in Flüssigkeiten," in Mitteilungen über Forschungsarbeiten auf dem Gebiete des Ingenieurwesens, Berlin, Heidelberg: Springer Berlin Heidelberg, 1913, pp. 1–41. 10.1007/978-3-662-02239-9_1.

[39] V. Gnielinski, New equations for heat and mass transfer in the turbulent flow in pipes and channels, NASA STI/recon technical report A 41 (1) (1975) 8–16.

[40] R. Charnay, R. Revellin, J. Bonjour, Discussion on the validity of prediction tools for two-phase flow pressure drops from experimental data obtained at high saturation temperatures, Int. J. Refrig 54 (2015) 98–125, https://doi.org/10.1016/j.ijrefrig.2015.02.014.

[41] M. Zhang, R.L. Webb, Correlation of two-phase friction for refrigerants in small-diameter tubes, Exp Therm Fluid Sci 25 (3–4) (2001) 131–139, https://doi.org/10.1016/S0894-1777(01)00066-8.

[42] D. Kim, S. Jeong, Effect of micro-grooves on the two-phase pressure drop of CO2 in a mini-channel tube, Int. J. Refrig 36 (8) (2013) 2040–2047, https://doi.org/10.1016/j.ijrefrig.2013.05.019.

[43] M. Ducoulombier, S. Colasson, J. Bonjour, P. Haberschill, Carbon dioxide flow boiling in a single microchannel – Part I: Pressure drops, Exp Therm Fluid Sci 35 (4) (2011) 581–596, https://doi.org/10.1016/j.expthermflusci.2010.12.010.

[44] Z. Liu, R.H.S. Winterton, A general correlation for saturated and subcooled flow boiling in tubes and annuli, based on a nucleate pool boiling equation, Int J Heat Mass Transf 34 (11) (1991) 2759–2766, https://doi.org/10.1016/0017-9310(91)90234-6.

[45] S.G. Kandlikar, P. Balasubramanian, An Extension of the Flow Boiling Correlation to Transition, Laminar, and Deep Laminar Flows in Minichannels and Microchannels, Heat Transfer Eng. 25 (3) (2004) 86–93, https://doi.org/10.1080/01457630490280425.

[46] S. Saitoh, H. Daiguji, E. Hihara, Correlation for boiling heat transfer of R-134a in horizontal tubes including effect of tube diameter, Int J Heat Mass Transf 50 (25–26) (2007) 5215–5225, https://doi.org/10.1016/j.ijheatmasstransfer.2007.06.019.

[47] F.T. Kanizawa, C.B. Tibiriçá, G. Ribatski, Heat transfer during convective boiling inside microchannels, Int J Heat Mass Transf 93 (2016) 566–583, https://doi.org/10.1016/j.ijheatmasstransfer.2015.09.083.

[48] R. Charnay, R. Revellin, J. Bonjour, Flow boiling heat transfer in minichannels at high saturation temperatures: Part II – Assessment of predictive methods and impact of flow regimes, Int J Heat Mass Transf 87 (2015) 653–672, https://doi.org/10.1016/j.ijheatmasstransfer.2015.03.080.

[49] R. Charnay, R. Revellin, J. Bonjour, Flow boiling characteristics of R-245fa in a minichannel at medium saturation temperatures, Exp Therm Fluid Sci 59 (2014) 184–194, https://doi.org/10.1016/j.expthermflusci.2014.01.011.

[50] R. Charnay, J. Bonjour, R. Revellin, Experimental investigation of R-245fa flow boiling in minichannels at high saturation temperatures: Flow patterns and flow pattern maps, Int J Heat Fluid Flow 46 (Apr. 2014) 1–16, https://doi.org/10.1016/j.ijheatfluidflow.2013.12.002.